AD-A107 854 DEFENCE RESEARCH ESTABLISHMENT VALCARTIER (QUEBEC) F/G 17/5
MULTIPLE TARGET TRACKING WITH AN AM RETICLE SEEKER (POURSUITE D--ETC(U)
SEP 81 K W MORGAN
UNCLASSIFIED DREV-R-4203/81 NL

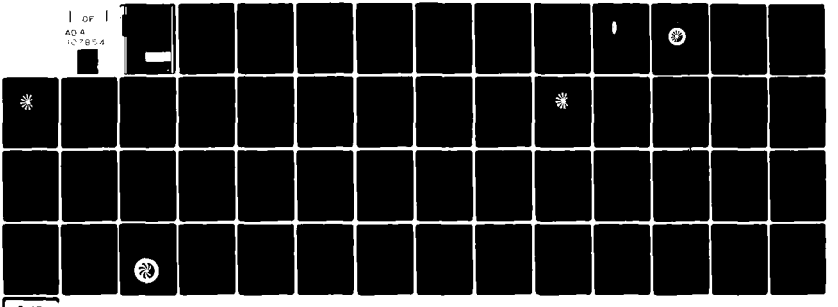

END
DATE FILMED
11-82
DTIC

UNCLASSIFIED
UNLIMITED DISTRIBUTION

CRDV RAPPORT 4203/81
DOSSIER: 3621J-013
SEPTEMBRE 1981

DREV REPORT 4203 81
FILE: 3621J-013
SEPTEMBER 1981

MULTIPLE TARGET TRACKING WITH AN AM RETICLE SEEKER

K.W. Morgan

Centre de Recherches pour la Défense
Defence Research Establishment
Valcartier, Québec

BUREAU - RECHERCHE ET DEVELOPPEMENT
MINISTERE DE LA DEFENSE NATIONALE
CANADA

RESEARCH AND DEVELOPMENT BRANCH
DEPARTMENT OF NATIONAL DEFENCE
CANADA

NON CLASSIFIÉ
DIFFUSION ILLIMITÉE

CRDV R-4203/81
DOSSIER: 3621J-013

UNCLASSIFIED

DREV-R-4203/81
FILE: 3621J-013

MULTIPLE TARGET TRACKING WITH AN AM RETICLE SEEKER

(Poursuite de Cibles Multiples par un Autodirecteur a Reticule AM),

K.W. Morgan

CENTRE DE RECHERCHES POUR LA DEFENSE
DEFENCE RESEARCH ESTABLISHMENT
VALCARTIER
Tel: (418) 844-4271

Québec, Canada

September/septembre 1981

NON CLASSIFIE

RESUME

On a conçu un modèle mathématique de réticule de tête chercheuse à modulation d'amplitude et déterminé sa position d'équilibre stable en présence d'une cible à double points, ou à simple point accompagnée d'une cible étendue. Le comportement de ce réticule constitue l'objet d'une simulation sur ordinateur numérique. (NC)

ABSTRACT

A generic AM-reticle seeker was modelled, and its steady-state equilibrium position, in the presence of either two point targets or a point and an extended target, determined by digital computer simulation. (U)

TABLE OF CONTENTS

LIST OF SYMBOLS

a_{ij}, b_{ij}	the j'th Fourier coefficients of the photocell signal from the i'th image
$a_j(x_k)$	value of a_j at the position x_k on the k curve
a_S	sum of a_{11} and a_{13}
c_j, d_j	the j'th Fourier coefficients of the signal following the automatic gain control
C(x,y)	Cartesian coordinates of target image position
C_X, C_Y	correction signals
E_X, E_Y	error signals
E'_X	error signal in X direction without automatic gain control
f_s	reticle spin frequency (Hz)
N	ratio of target image intensities
p	number of pairs of opaque and transparent sectors
$P(r,\psi)$	polar coordinates of target image position
r	distance of target image from reticle centre
RMS	root mean square value
S(AGC)	filtered signal after automatic gain control
S(F)	total filtered signal
$S(F_i)$	filtered signal from the i'th point target image
t	time (s)
x_L	position of line target image
x_P	position of point target image
α	$\omega_s \cdot t$
β	arcsin r
ψ	argument defining the target image position in polar coordinates
Λ	half-arc length of target image
ω_s	reticle spin rate (rad/s)

1.0 INTRODUCTION

An infrared seeking missile employs the radiation from the target as its homing source; its gimballed seeker head precesses to follow this source. Although there has been a rapid development of charge-coupled devices suitable for processing target radiation, current threats are more likely to use mechanical scanning. The mechanical scanners, which have fields of view of a little more than a degree to several degrees, are either of the rosette or reticle types. The rosette-type scans with a very narrow instantaneous field of view, thus permitting the recognition of individual characteristics. The reticle scanners include those which provide pulse-position modulation, frequency modulation or amplitude modulation to encode the angular position of the target relative to the seeker axis. In this document a seeker employing an amplitude-modulating (AM) reticle is examined; related reticles are employed in certain American and Soviet missiles.

With two targets within its field of view, the seeker of a missile employing an AM reticle has a tendency to point nearer to the more intense one, a property which is employed to decrease the effectiveness of the infrared seeking missile; a target can dispense a decoy flare, which, if it is sufficiently intense, may be accepted by the missile seeker as a preferential source of radiation to the target itself. Analyses of infrared decoy flare effectiveness require the determination of the position to which the seeker of the attacking missile will point relative to the target and flare positions. To simplify the calculations, it is often assumed that the seeker will point to the weighted mean, that is: the product of image intensity and distance from the centre of the reticle will in the steady state be

equal for the target and the flare. This assumption may be valid when two infrared sources are far from the missile, and the images on the reticle are thus small. But it will no longer be true as the missile approaches the targets, and the images occupy a substantial portion of the reticle.

A model of a generic AM seeker is developed, and its performance examined for certain specific cases which are tractable by exact mathematical solutions. As well as introducing the reader to the seeker behaviour, these examples serve to validate the computer programme. A digital programme is developed from the model, and employed to determine the seeker equilibrium in the presence of two point targets as a function of target separation and relative target intensities. This is then extended to include the case where one target is an extended source. The results may be of assistance in the modelling required for flare-effectiveness studies.

This report covers the work performed at DREV between 1 October 1979 and 1 August 1980 under PCN 21J13, "Multiple Target Tracking with a Reticle Seeker".

2.0 MODEL

2.1 General

A generalized schematic of an infrared seeker is shown in Fig. 1. The infrared emission from the target is focussed onto a reticle spinning about its centre at a frequency of f_s. The reticle consists of alternate opaque and transparent sectors, which chop the incident radiation to produce a carrier of frequency $p.f_s$ at the photocell output, where p is the number of pairs of opaque and transparent sectors. The chopping efficiency is maximum for an image capable of being instantaneously masked or unmasked totally; such image can be either a point or a straight line (or its extension) passing through the centre of the reticle. This waveform is modulated at the spin frequency by a semi-transparent phasing sector. An automatic gain control (AGC) keeps the amplitude of the carrier constant and independent of the target intensity, which is a requirement for linear control. This signal is demodulated and produces quadrature components at the spin frequency, the amplitudes of which are a measure of the angular error between the look angle of the seeker and a line to the target. These error signals are applied, via torquing motors, to precess the reticle assembly to reduce the error angle to a small value.

2.2 Reticle

The reticle used in this model is shown in Fig. 2. It possesses twelve pairs of transparent and opaque spokes, and the inner boundaries of the phasing sector are delimited by semi-circles, centred on opposite sides of a diameter of the reticle, the radiuses of which are half that

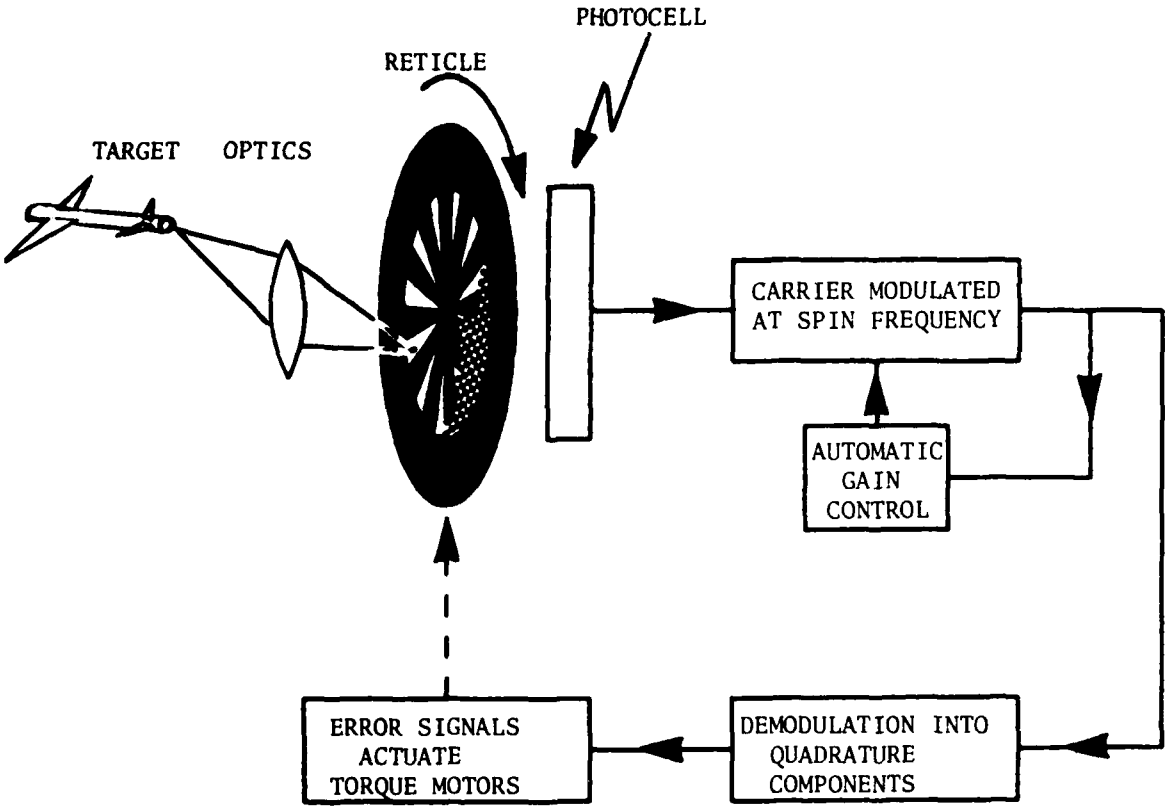

FIGURE 1 - Control system

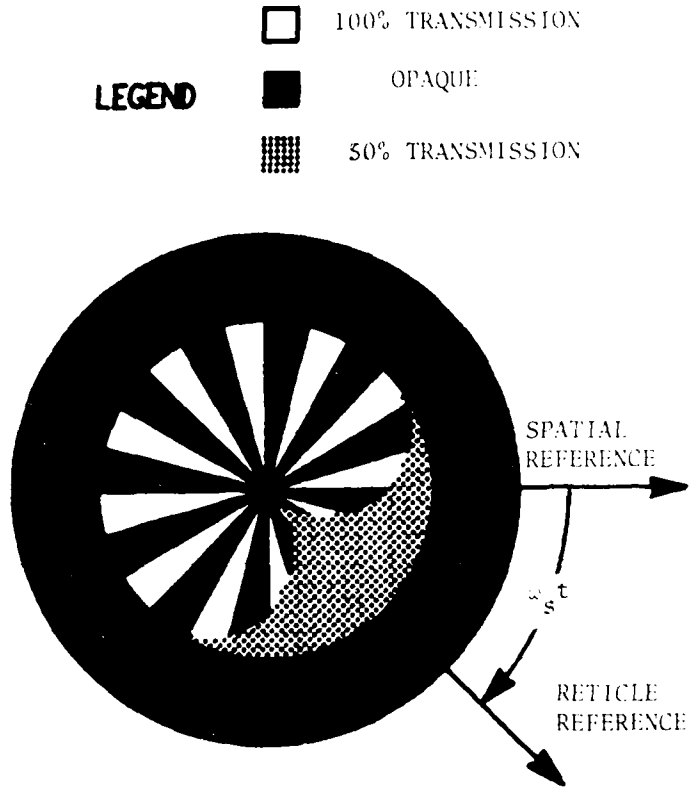

FIGURE 2 - The reticle

of the reticle. The phasing sector has a transmission of 50%, so that the average signal will be the same during image dwell on the phasing sector and image dwell on the spokes; this will tend to improve discrimination against large images. Harmonic reference signals are generated at the spin frequency of the reticle, which rotates in a clockwise direction at a rate of ω_s rad/s.

To illustrate the manner in which the reticle encoding is used to produce error signals, an example is now given in which, for ease of comprehension, the signal processing is greatly simplified. Let the target image be at a distance r from the centre of the reticle. Then, from the reticle geometry given in Fig. 3, it can be seen that the image will be interrupted by the phasing sector for an angle of 2 arcsin r(=2β) for each rotation of the reticle. For this particular figure only, the image has been rotated around the centre of the stationary reticle.

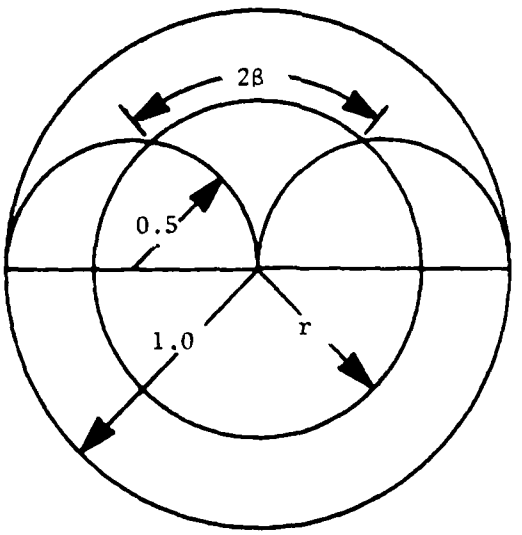

FIGURE 3 - Reticle geometry

Suppose that the image is at $P(r,\psi)$, as shown in Fig. 4(a), which has been drawn for the instant that the reticle and spatial references are coincident. The photocell signal will then be as in Fig. 4(b) Reference signals (Fig. 4(c)) are generated by the reticle motor, and are phased so that the information contained in the photocell signal can be correctly recovered. The photocell signal is rectified (Fig. 4(d)) and, in conjunction with the reference signals, its SINE and COSINE components are determined.

$$\text{COSINE} = \frac{1}{\pi}\left[\int_{0}^{2\pi-\beta-\psi} \cos\alpha \, d\alpha + \int_{2\pi+\beta-\psi}^{2\pi} \cos\alpha \, d\alpha\right],$$

$$= -\frac{2}{\pi} \sin\beta \cos\psi \,, \qquad [1]$$

$$= -\frac{2}{\pi} r \cos\psi \,,$$

where

$$\alpha = \omega_s t \,.$$

Similarly

$$\text{SINE} = \frac{2}{\pi} r \sin\psi \,. \qquad [2]$$

The spatial axes are defined such that when $\psi = 0$, the image lies on the positive X axis, and when $\psi = \pi/2$, it lies on the positive Y axis. It is required that, when an error is in the positive direction, the error signal be also positive. For this to occur, the error signals for the X and Y directions (E_X and E_Y) must be equal to (-COSINE) and SINE respectively, which requires the use of (-cosine) and sine reference signals. Henceforth, these will be the reference signals employed.

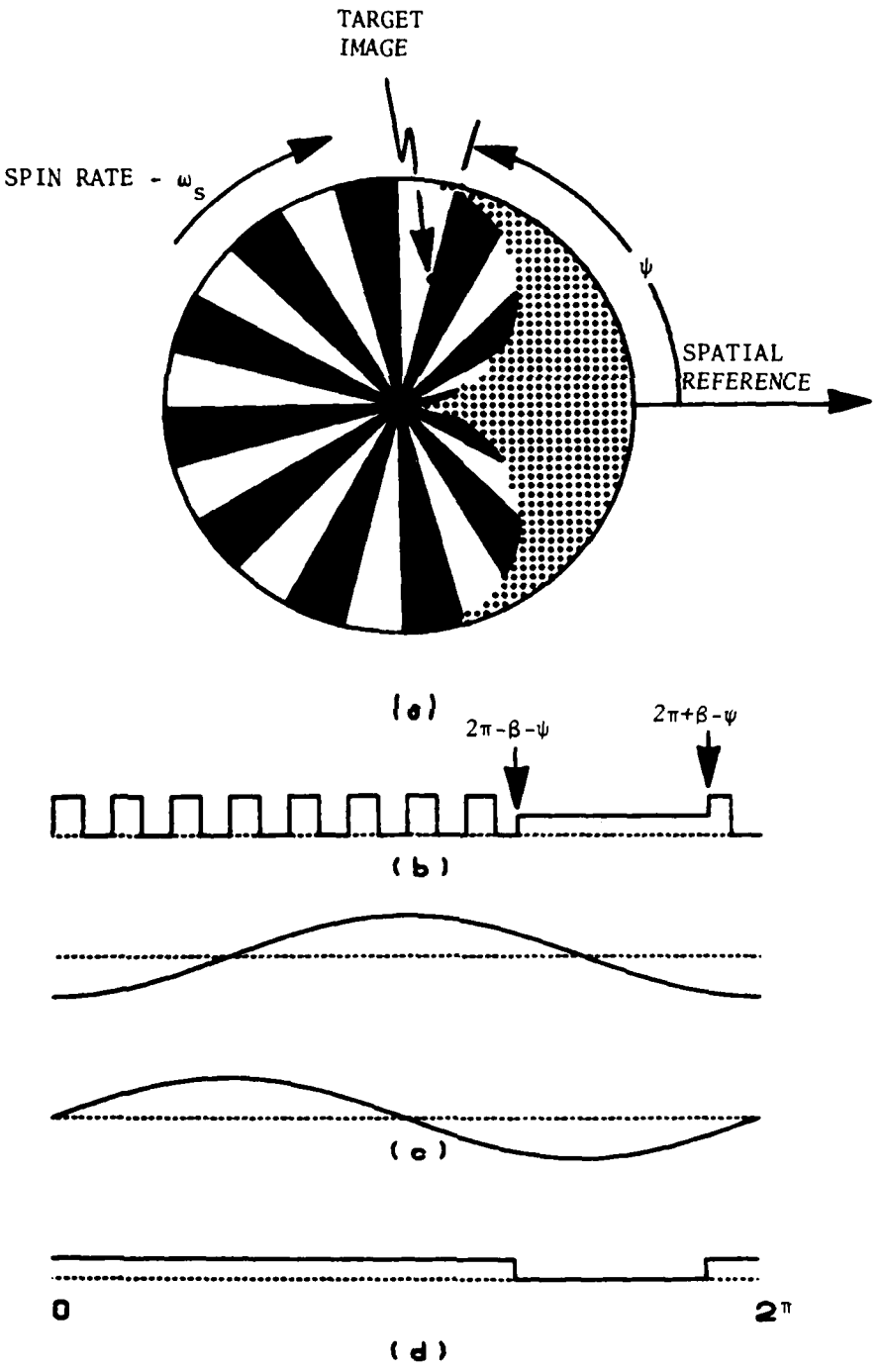

FIGURE 4 - Waveforms required for example

As this simplified example demonstrates a linear control it would be anticipated that the more sophisticated model, which is employed throughout the remaining analyses, will show a similar tendency.

2.3 Signal Processing

The photocell signal is first filtered. In the model, only the carrier (at the spoke frequency) and its immediate side-bands are passed by the filter. If the spin frequency is f_s, that of the carrier will be $12f_s$ (assuming a 12-spoke reticle), and the filter will pass only components at $11f_s$, $12f_s$ and $13f_s$. In practice, the signals from the various target images are summed by the photocell, and then filtered. As the signal processing to this point is linear, the model achieves the same result by filtering the signals from the individual images, and then summing. Thus the filtered signal from the i'th image can be represented by

$$S(F_i) = \sum_{j=11}^{13} (a_{ij} \sin j\alpha + b_{ij} \cos j\alpha) \quad . \qquad [3]$$

The total filtered signal is then

$$S(F) = \sum_{i} S(F_i) \quad . \qquad [4]$$

Before this signal is detected, some form of automatic gain control must be applied, otherwise the amplitude of the error signals will be a function of the image intensities, and linear control would not be feasible. The type of AGC employed herein, is that of dividing S(F) by its root-mean-square (RMS) value, to give

$$S(AGC) = S(F)/RMS, \qquad [5]$$

where

$$RMS = \left[\sum_{j=11}^{13} (a_j^2 + b_j^2) \right]^{\frac{1}{2}} , \qquad [6]$$

and $a_j = \sum_i a_{ij}$; $b_j = \sum_i b_{ij}$.

This signal is then square-law detected, and the coefficients of sin α and cos α extracted. Let

$$S(AGC) = \sum_{j=11}^{13} (c_j \sin j\alpha + d_j \cos j\alpha) . \qquad [7]$$

Then

$$S^2(AGC) = E_X \cos \alpha + E_Y \sin \alpha + \text{higher frequency components}, \qquad [8]$$

where

$$E_X = -(c_{12}(c_{11} + c_{13}) + d_{12}(d_{11} + d_{13})) ,$$

$$E_Y = c_{12}(d_{11} - d_{13}) - d_{12}(c_{11} - c_{13}).$$

The higher frequency components are filtered out, and E_X and E_Y are used to drive the reticle assembly, in the X and Y directions respectively, via the torque motors which have a gain of G.

A flowchart of the model is given in Fig. 5.

2.4 Error Signal for Small Error

If the target image is displaced only a small distance from the reticle centre, then sine and cosine approximations can be employed to simplify the calculations. This will permit a further example of the signal processing to be given, without as yet resorting to a computer. In Fig. 6(a) is shown the photocell signal for a target image on the X

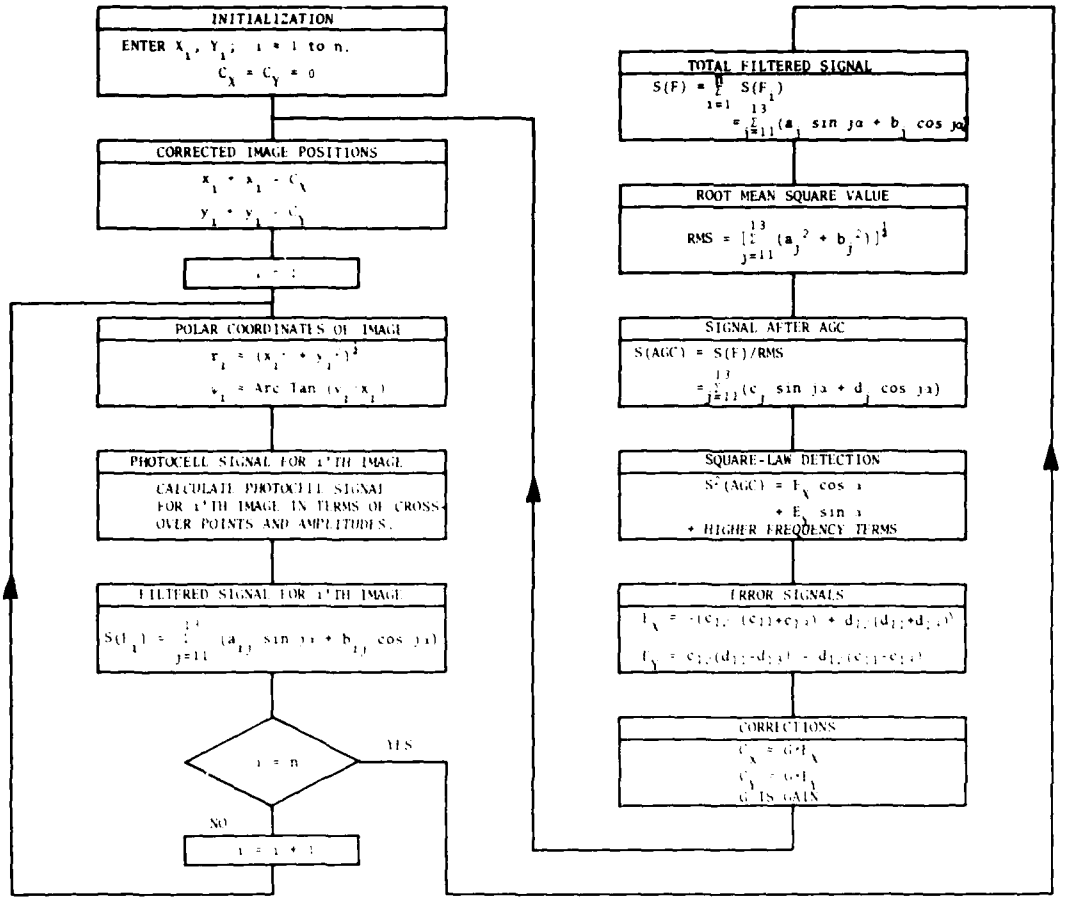

FIGURE 5 - Flowchart of seeker model

axis at a distance r from the reticle centre, where r is much smaller than π/p, and p is the number of pairs of sectors (=12).

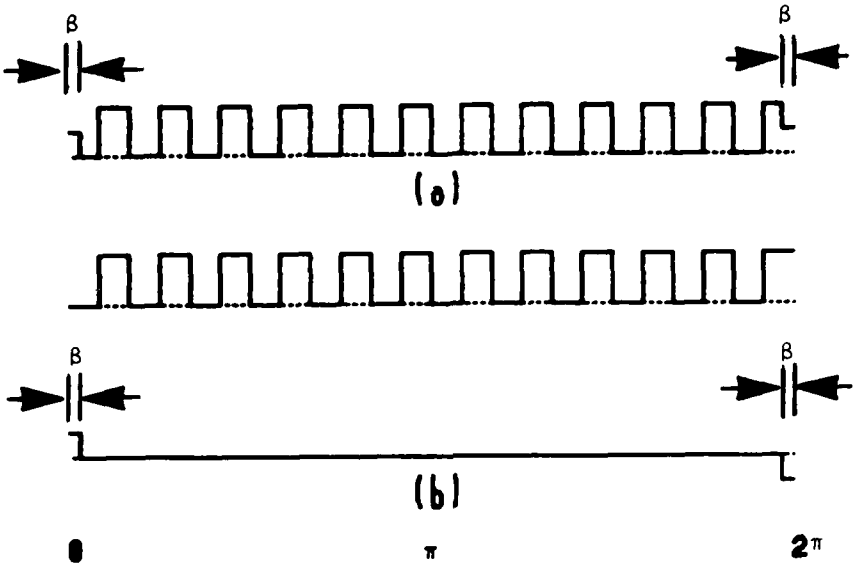

FIGURE 6 - The photocell waveform

The filtered signal then has the following form

$$S(F) = \sum_{i=-1}^{1} [a_{p+i}\sin(p + i)\alpha + b_{p+i}\cos(p + i)\alpha]. \qquad [9]$$

The equation will now be written in the following tabular form

$$S(F) = \begin{vmatrix} u_{-1} & u_0 & u_1 \\ v_{-1} & v_0 & v_1 \end{vmatrix} \qquad [10]$$

where u_n is the coefficient of $\sin(n + p)\alpha$,

and v_n is the coefficient of $\cos(n + p)\alpha$; $n = -1, 0, 1$,

and the straight-line brackets are a function which performs the following operation

$$\sum_{-1}^{1} u_n \sin(n + p)\alpha + v_n \cos(n + p)\alpha.$$

The waveform of Fig. 6(a) will be analysed by first separating it into the two parts shown in Fig. 6(b). It follows that the S(F) for the photocell signal is

$$S(F) = \left| \begin{matrix} \dfrac{1 - \cos(p-1)\beta}{(p-1)\pi} & \dfrac{-2}{\pi} + \dfrac{1 - \cos p\beta}{p\pi} & \dfrac{1 - \cos(p+1)\beta}{(p+1)\pi} \\ 0 & 0 & 0 \end{matrix} \right| . \quad [11]$$

Assume $pr \ll 1$, so that $\beta = (\arcsin r) \approx r$, then eq. 11 can be written

$$S(F) = \left| \begin{matrix} \dfrac{(p-1)\, r^2}{2\pi} & -\dfrac{2}{\pi} & \dfrac{(p+1)\, r^2}{2\pi} \\ 0 & 0 & 0 \end{matrix} \right| . \quad [12]$$

Let the target image be displaced from C(x,0), or P(r,0), to C(x,y), or P(r,ψ), where

$$r = (x^2 + y^2)^{\frac{1}{2}} ,$$

$$\psi = \text{Arctan } y/x .$$

In the model the phase angle is introduced after the filtering, so that

$$S(F) = \left| \begin{matrix} \dfrac{(p-1)}{2\pi}\, r^2 \cos(p-1)\psi & -\dfrac{2}{\pi} \cos p\psi & \dfrac{(p+1)}{2\pi}\, r^2 \cos(p+1)\psi \\ \dfrac{(p-1)}{2\pi}\, r \sin(p-1)\psi & -\dfrac{2}{\pi} \sin p\psi & \dfrac{(p+1)}{2\pi}\, r^2 \sin(p+1)\psi \end{matrix} \right| . \quad [13]$$

In the case of multiple targets, it is at this point that the $S(F_i)$ would be summed to form S(F). The RMS value, because r is small, is very close to $2/\pi$. Hence

$$S(AGC) = \begin{vmatrix} \frac{(p-1)}{4} r^2\cos(p-1)\psi & -\cos p\psi & \frac{(p+1)}{4} r^2\cos(p+1)\psi \\ \frac{(p-1)}{4} r^2\sin(p-1)\psi & -\sin p\psi & \frac{(p+1)}{4} r^2\sin(p+1)\psi \end{vmatrix} . \quad [14]$$

Equation 14 is substituted in eq. 8 to give

$$E_X = \frac{r^2}{4} \{\cos p\psi[(p-1)\cos(p-1)\psi + (p+1)\cos(p+1)\psi] + \sin p\psi [(p-1)\sin(p-1)\psi + (p+1)\sin(p+1)\psi]\} \quad [15]$$

$$= 6\, r^2\cos\psi$$

$$E_Y = \frac{-r^2}{4} \{\cos p\psi [(p-1)\sin(p-1)\psi - (p+1)\sin(p+1)\psi] - \sin p\psi [(p-1)\cos(p-1)\psi - (p+1)\cos(p+1)\psi]\} \quad [16]$$

$$= 6\, r^2\sin\psi$$

It is seen that for small displacements the system has a square-law control.

2.5 Equilibrium Position for Two Targets (Small Displacement)

A further example is now given where two targets are present, but with only a small separation between them. Let the first target have an intensity of unity and a position at equilibrium of $C(x_1,0)$, and the other target an intensity of N and a position at equilibrium of $C(-x_2,0)$. Then if $px_1(x_2)<<1$, by applying eq. 12 to both targets, the

filtered photocell signal is

$$S(F) = \begin{vmatrix} \frac{(p-1)}{2\pi}(x_1^2 - Nx_2^2) & -\frac{2}{\pi}(N+1) & \frac{(p+1)}{2\pi}(x_1^2 - Nx_2^2) \\ 0 & 0 & 0 \end{vmatrix} . \qquad [17]$$

For equilibrium E_x must be zero (refer to eq. 8), that is

$$2\frac{(N+1)}{\pi^2}p(x_1^2 - Nx_2^2) = 0, \qquad [18]$$

the solution of which is

$$\frac{x_1}{x_2} = N^{\frac{1}{2}} . \qquad [19]$$

This is to be expected from the square-law relationship between the error signal and the image error (r) derived in Section 2.4. This position can be seen to be stable, as eq. 18 shows that an increase of x_1, with a consequent decrease in x_2, will cause E_x to become positive, whereas if x_1 becomes negative so does E_x. A positive error signal will cause the reticle to move to the right and hence decrease the error (x_1) between the reticle centre and a target image lying to the right of centre.

2.6 Extended Target

First consider the case where two targets, at the same distance from the centre, are separated by the width of one sector, as shown in Fig. 7(a), which has been illustrated to show the instant at which the reticle and spatial references are coincident. The waveforms resulting from the two individual images are shown in Fig. 7(b), and the total signal in Fig. 7(c), where ψ_A and ψ_B are the arguments of the positions of images A and B.

An analysis of the waveform of Fig. 7(c), which is given in Appendix A, shows that

$$\int_0^{2\pi} \sin p\alpha \cdot f(A+B)\, d\alpha = \int_0^{2\pi} \cos p\alpha \cdot f(A+B)\, d\alpha = 0 \quad . \qquad [20]$$

and thus $a_{12} = b_{12} = 0$; it can be seen, from eq. 8, that because of this the error signal will also be zero. It follows that if the target image was in the form of an arc, covering more than one sector, the carrier signals from all points separated by exactly one sector's width would nullify one another. If the arc was to cover exactly an even number of sectors, the carrier would be lost, and the error signal would be zero.

The signals from an arc image will now be examined. An arc is chosen as an image shape, in preference say to a straight line, only because of its mathematical simplicity in this introductory analysis. It suffers from the disadvantage that nothing can be concluded about the stability of equilibrium positions, as once the image moves it is no longer an arc with the same centre, and hence the equations employed in the analysis become invalid.

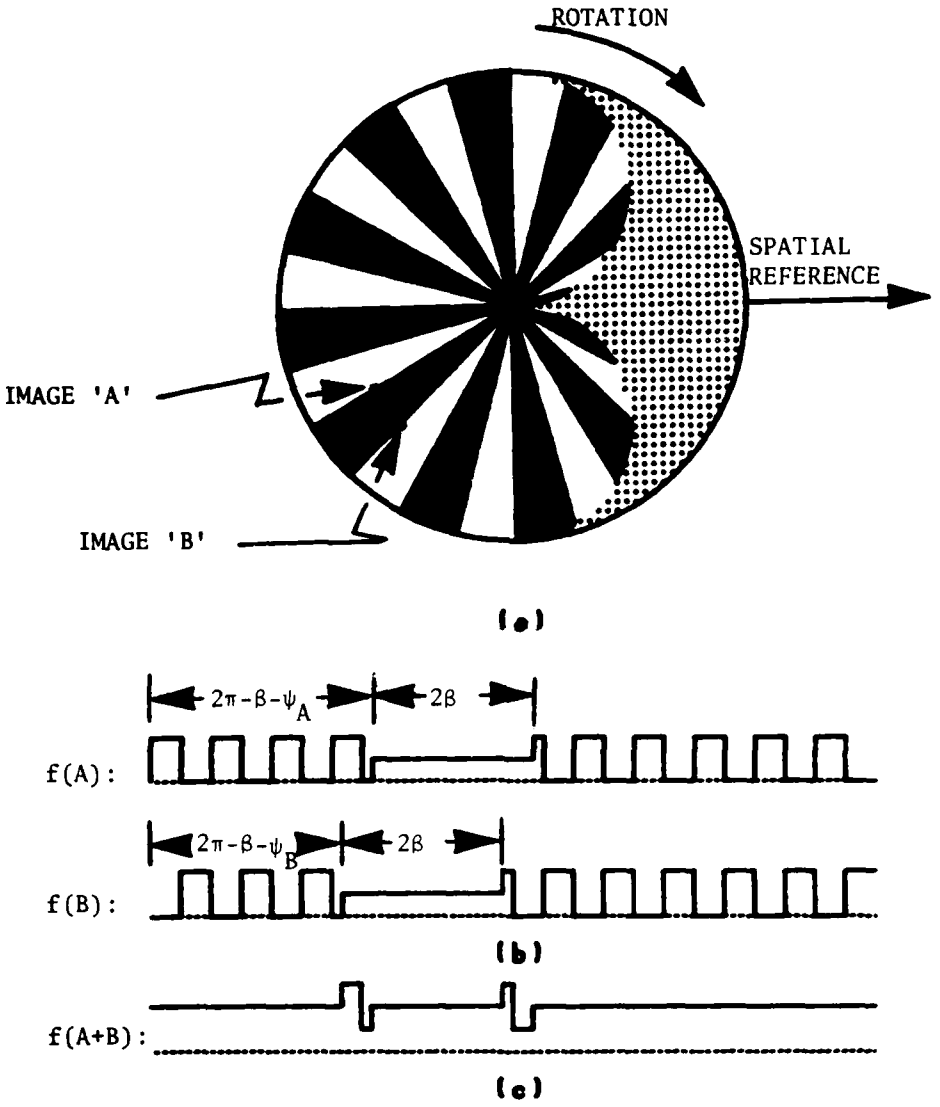

FIGURE 7 - Waveforms from two images

In Fig. 8(a), the target image is shown by a heavy arc from $P(1,-\Lambda)$ to $P(1,\Lambda)$. To derive the error signals resulting from this image, the filtered signal for an image of unit intensity situated at $P(1,0)$ will first be calculated. Its photocell signal is shown in Fig. 8(b), and hence (see also Appendix B)

$$S(F) = \begin{vmatrix} u_{11} & u_{12} & u_{13} \\ 0 & 0 & 0 \end{vmatrix}, \qquad [21]$$

where

$$u_{11} = 7.596/11\pi,$$
$$u_{12} = -1/\pi,$$
$$u_{13} = 7.596/13\pi.$$

If the intensity of the arc is uniform, and its total radiance is unity, then for a segment at $P(1,\lambda)$ of length $\delta\lambda$

$$S(F_{\delta\lambda}) = \frac{\delta\lambda}{2\Lambda} \begin{vmatrix} u_{11}\cos 11\lambda & u_{12}\cos 12\lambda & u_{13}\cos 13\lambda \\ u_{11}\sin 11\lambda & u_{12}\sin 12\lambda & u_{13}\sin 13\lambda \end{vmatrix}. \qquad [22]$$

In the limit

$$S(F) = \int_{-\Lambda}^{\Lambda} S(F_{d\lambda}) \quad \text{as} \quad \delta\lambda \to d\lambda \to 0,$$
$$= \frac{1}{\Lambda} \begin{vmatrix} \frac{u_{11}}{11}\sin 11\Lambda & \frac{u_{12}}{12}\sin 12\Lambda & \frac{u_{13}}{13}\sin 13\Lambda \\ 0 & 0 & 0 \end{vmatrix}. \qquad [23]$$

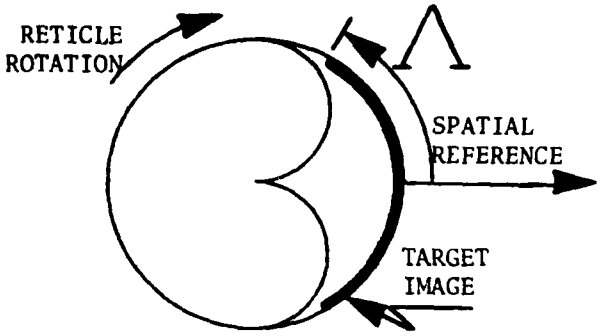

(a)

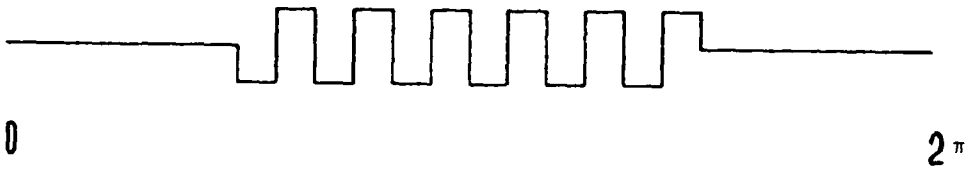

(b)

FIGURE 8 - Extended target

The carrier amplitude of the arc is

$$a_{12} = (\sin 12\Lambda)/12\pi\Lambda, \qquad [24]$$

and the sum of the side-band amplitudes is

$$a_S = \frac{7.596}{\pi\Lambda}\left(\frac{\sin 11\Lambda}{11^2} + \frac{\sin 13\Lambda}{13^2}\right). \qquad [25]$$

These are plotted in Fig. 9. As the peaks of both the carrier and the sum of the side-bands decrease rapidly with arc length, their contribution to the total error signal, in the presence of a point source of similar intensity, will be very small.

Further, an arc of total length say π would be in equilibrium, as the carrier amplitude is then zero. A point image at the centre of the reticle is also in equilibrium, and eq. 12 shows that this is because the side-band amplitudes are zero. However, if both the arc and point images are present at the same time, the seeker is no longer in equilibrium, as the side-bands from the arc and the carrier from the point will generate an error signal and cause a displacement of the seeker.

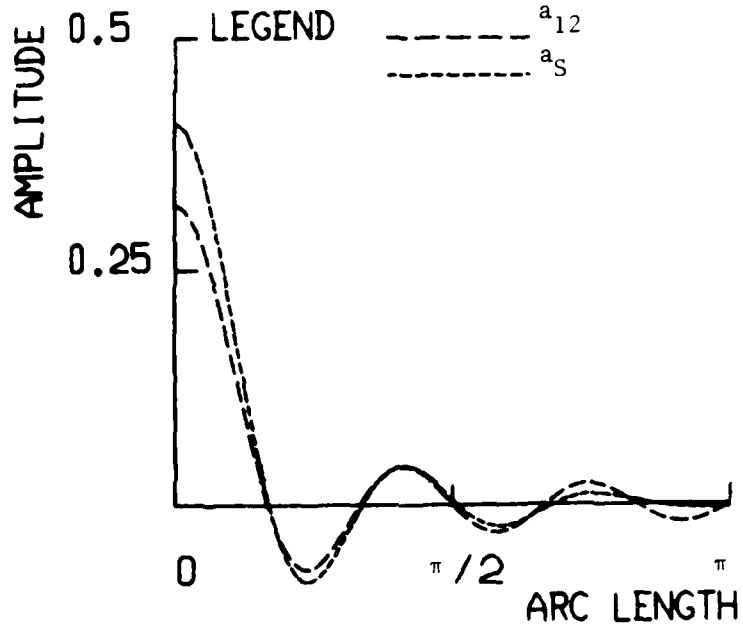

FIGURE 9 - Amplitudes of carrier and side-bands as a function of arc length

3.0 RESULTS

3.1 General

The preceding analyses have served either to illustrate the functioning of the seeker or to provide a means of validating the computer programme, and as such have investigated special cases or used approximations. The rest of the study, which will be general, will require the use of a digital computer. The simulation model was programmed in APL, and run on the Xerox 560 digital computer. The programmes are listed in Appendix C.

3.2 Error Curves

The error curve (Fig. 10(a)) gives the error signal as a function of the distance of a point image from the centre of the reticle. It is to be noted that the curve gives an overall appearance of linearity, as was suggested by the reasoning in Section 2.2. The number of peaks on the curve corresponds to the number of changes of spoke interceptions with the phasing sector as r varies from 0 to 1.

Figure 10(b), which is plotted from the data of Table I, shows the portion of the error curve for small values of r. In Section 2.4 the error signal was derived as being equal to $6r^2$ for values of r less than 0.08; this verifies that the part of the error curve for small values of r is correct.

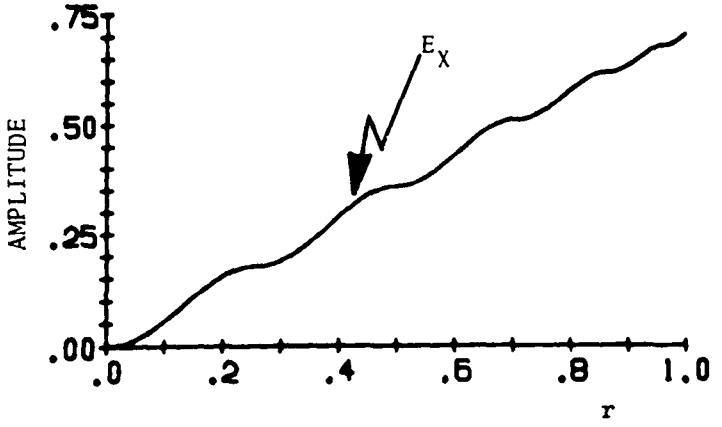

(a)

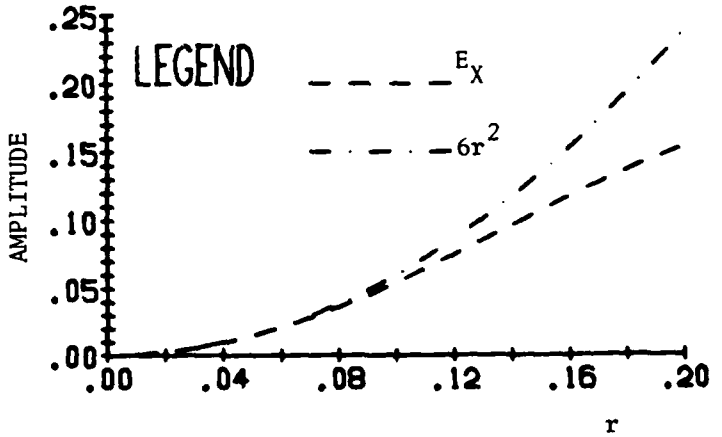

(b)

FIGURE 10 - Error curve

TABLE I

Error signal for small r

r	E_x	$6r^2$
0.01	0.000599	0.0006
0.02	0.00239	0.0024
0.03	0.00536	0.0054
0.04	0.00946	0.0096
0.05	0.0147	0.015
0.06	0.0209	0.0216
0.07	0.0281	0.0294
0.08	0.0362	0.0384
0.09	0.045	0.0486
0.1	0.0545	0.06
0.11	0.0646	0.0726
0.12	0.075	0.0864
0.13	0.0857	0.101
0.14	0.0965	0.118
0.15	0.107	0.135
0.16	0.118	0.154
0.17	0.128	0.173
0.18	0.137	0.194
0.19	0.146	0.217
0.2	0.154	0.24

3.3 Equilibrium Position for Two Point Targets

In this test, two point target images are placed at a given distance apart and, after equilibrium has been reached, their distances from the reticle centre are noted. The two images are situated at $C(x_1,0)$ and $C(x_2,0)$, with intensities of 1 and N. The images are a fixed distance apart (d), where $d = x_1 - x_2$.

From Fig. 11 and Table II it can be seen for $d = 0.001$ that

$$\log N\,|x_2/x_1| = \tfrac{1}{2}\log N,$$

or

$$|x_1/x_2| = N^{\frac{1}{2}}. \qquad [26]$$

This result is in agreement with eq. 19.

For larger d the value of $N|x_2/x_1|$ is close to unity, that is $|x_1/x_2| \approx N$, if neither image is close to the centre of the reticle, so that a weighted mean can be applied in this case to calculate the equilibrium position. Once either of the images is close to the reticle centre, the signals from this image will no longer be linearly proportional to its distance from the centre; nevertheless, the slopes of the curves for large N remains one half.

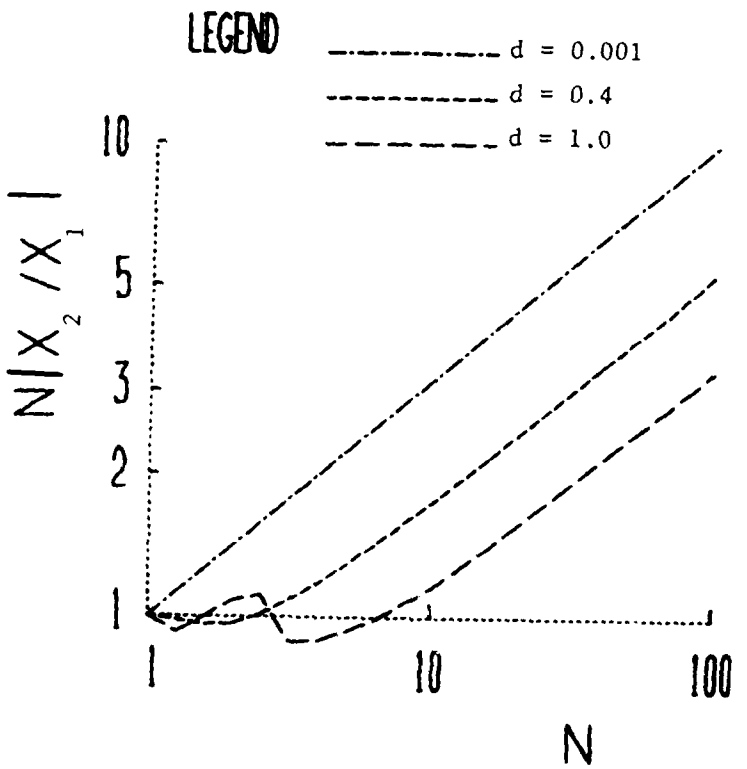

FIGURE 11 - Two point targets

TABLE II

Two point images

N	x_1	x_2	$\lvert x_1/x_2 \rvert$	$N\lvert x_1/x_2 \rvert$
d = 0.001				
1.00	.00050	-.00050	1.00	1.00
1.58	.00056	-.00044	1.26	1.26
2.51	.00061	-.00039	1.58	1.59
3.98	.00067	-.00033	1.99	2.00
6.31	.00072	-.00028	2.51	2.51
10.00	.00076	-.00024	3.16	3.16
15.85	.00080	-.00020	3.98	3.98
25.12	.00083	-.00017	5.01	5.01
39.81	.00086	-.00014	6.31	6.31
63.10	.00089	-.00011	7.94	7.94
100.00	.00091	-.00009	10.00	10.00
d = 0.4				
1.00	.200	-.200	1.00	1.00
1.26	.225	-.175	1.28	.98
1.58	.249	-.151	1.64	.97
2.00	.269	-.131	2.07	.97
2.51	.285	-.115	2.48	1.01
3.16	.298	-.102	2.92	1.08
3.98	.309	-.091	1.00	3.98
5.01	.318	-.082	3.89	1.29
6.31	.326	-.074	4.44	1.42
10.00	.340	-.060	5.72	1.75
15.85	.352	-.048	7.33	2.16
25.12	.361	-.039	9.31	2.70
39.81	.369	-.031	11.78	3.38
63.10	.375	-.025	15.00	4.21
100.00	.380	-.020	18.80	5.32
d = 1.0				
1.00	.500	-.500	1.00	1.00
1.26	.576	-.424	1.36	.93
1.58	.613	-.397	1.59	1.00
2.00	.649	-.351	1.85	1.03
2.51	.693	-.307	2.26	1.11
3.16	.781	-.219	3.56	.89
3.98	.817	-.183	4.45	.89
5.01	.843	-.157	5.37	.93
6.31	.865	-.135	6.41	.98
10.00	.897	-.103	8.67	1.15
15.85	.919	-.081	11.29	1.40
25.12	.935	-.065	14.48	1.73
39.81	.949	-.051	18.49	2.15
63.10	.959	-.041	23.57	2.68
100.00	.968	-.032	30.06	3.33

3.4 Representation of Line Targets

For various numbers of points forming the line-target image, the values of a_{11}, a_{12} and a_{13} are calculated and presented in Table III and Fig . 12, where the line is 0.8 long and positioned symmetrically about the X axis at x = 0.5. It was concluded from the figure that little error should occur by employing 21 points.

To verify that this number of points is sufficient to represent a line image anywhere on the X axis, the amplitudes of the carrier and the sum of the side-band amplitudes were plotted for the same line image, and its position along the X axis was varied from -1.0 to 1.0. The graph is given in Fig. 13 for a line image represented by 21 points and in Fig. 14 for 41 points. The only discernable difference between the two curves is in the peaks of the carrier immediately on either side of the ordinate.

TABLE III

Number of points to form a line image

Image length = 0.8 (Symmetrical about X axis),

Position of image: x = 0.5 .

NUMBER OF POINTS	a_{11}	a_{12}	a_{13}
1	.1099	-.5305	.0929
3	.0816	-.4953	.1065
7	.0232	-.0882	.0113
11	.0219	-.0821	.0100
21	.0213	-.0792	.0094
31	.0212	-.0786	.0093
51	.0211	-.0783	.0093
101	.0211	-.0782	.0092

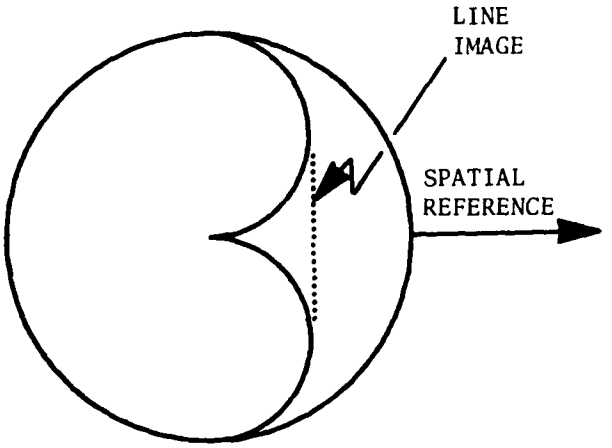

(a)

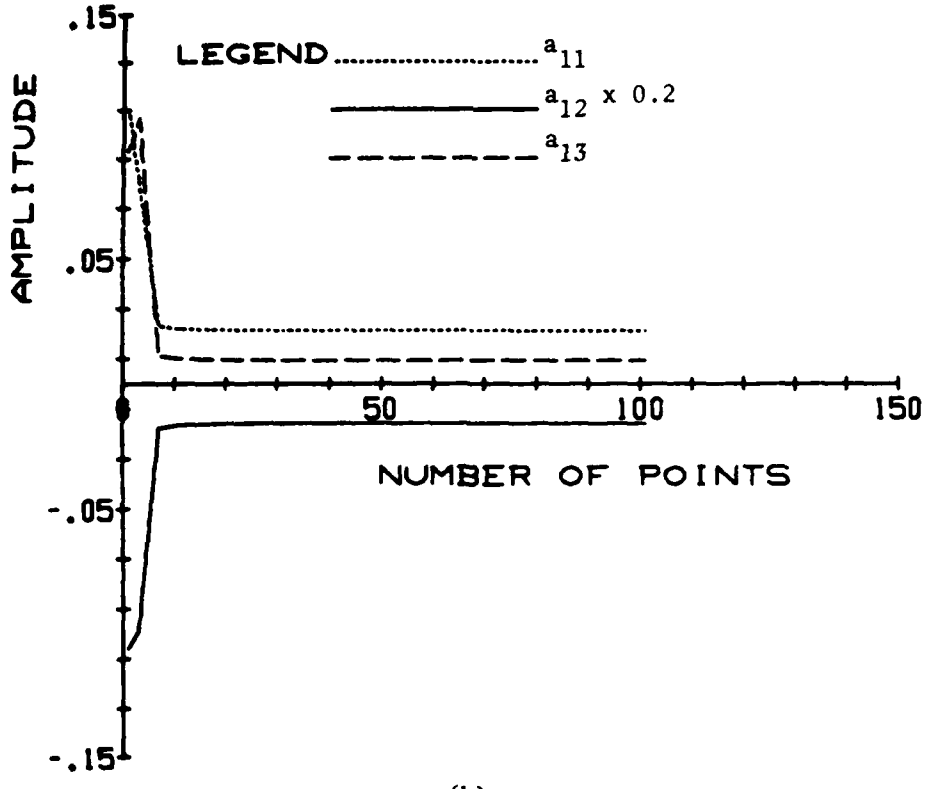

(b)

FIGURE 12 - Number of points to represent a line image

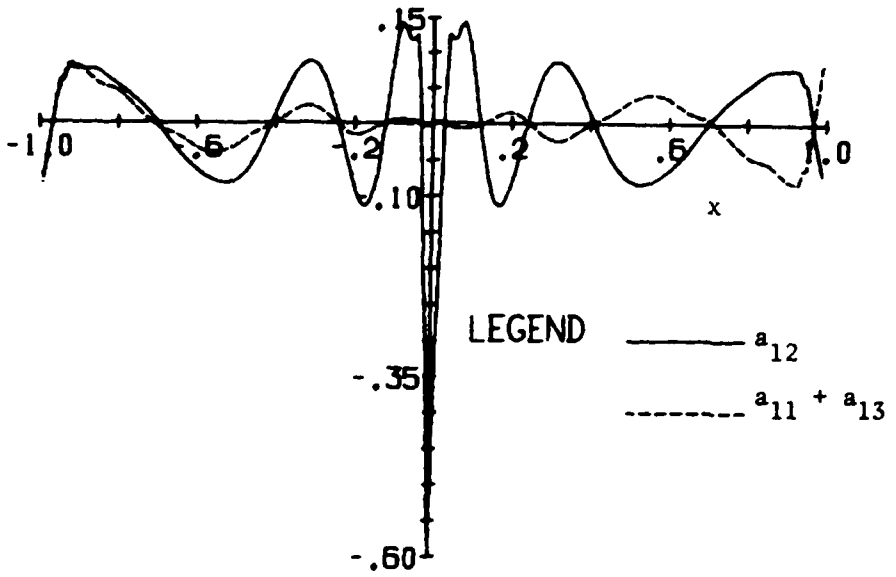

FIGURE 13 - Line signals for 21 points

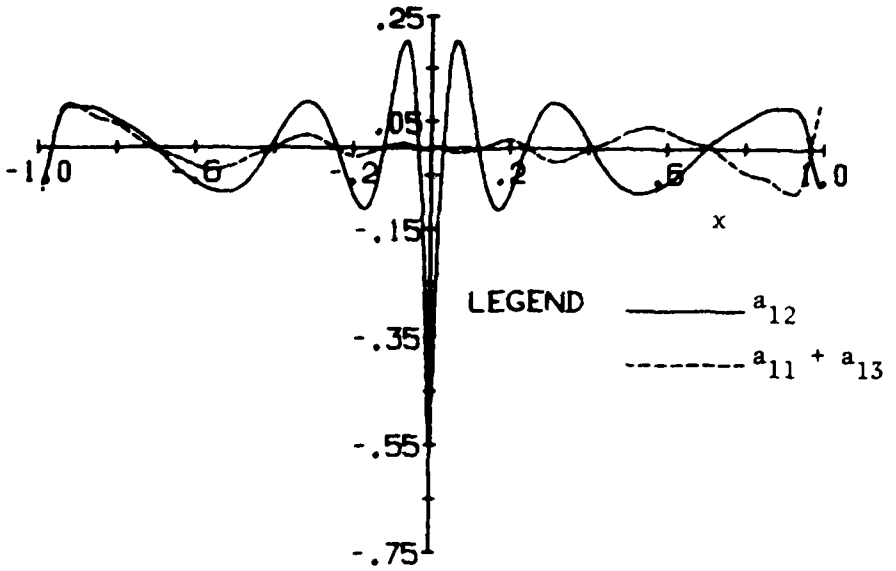

FIGURE 14 - Line signals for 41 points

3.5 Equilibrium Position in the Presence of a Line and a Point Target

The difference between the signals from the representation of a straight-line image by 21 and 41 points, as shown in Figs. 13 and 14, is small, and hence the following computations have been done with 21 points; the effect of the difference, if any, will be discussed at the end of this section.

In Figs. 15(a)-17(a) are shown the values of a_{12} and $a_S (= a_{11} + a_{13})$ for a point image of intensity N and a line image of unit intensity and of length 0.8 centred about the X axis. It is now required to derive the points of equilibrium from these curves for a given separation of the two images. The separation will be taken to be 0.5, with the point image lying to the left of the line image. For equilibrium to occur the error signal must be zero, that is

$$[a_{12}(x_P) + a_{12}(x_L)]\,[a_S(x_P) + a_S(x_L)] = 0 \ , \qquad [27]$$

where

x_P is the position of the point image,

x_L is the position of the line image,

$a_j(x_k)$ is the value of a_j at the point x_k on the k curve,

and

$$x_L - x_P = 0.5 \ .$$

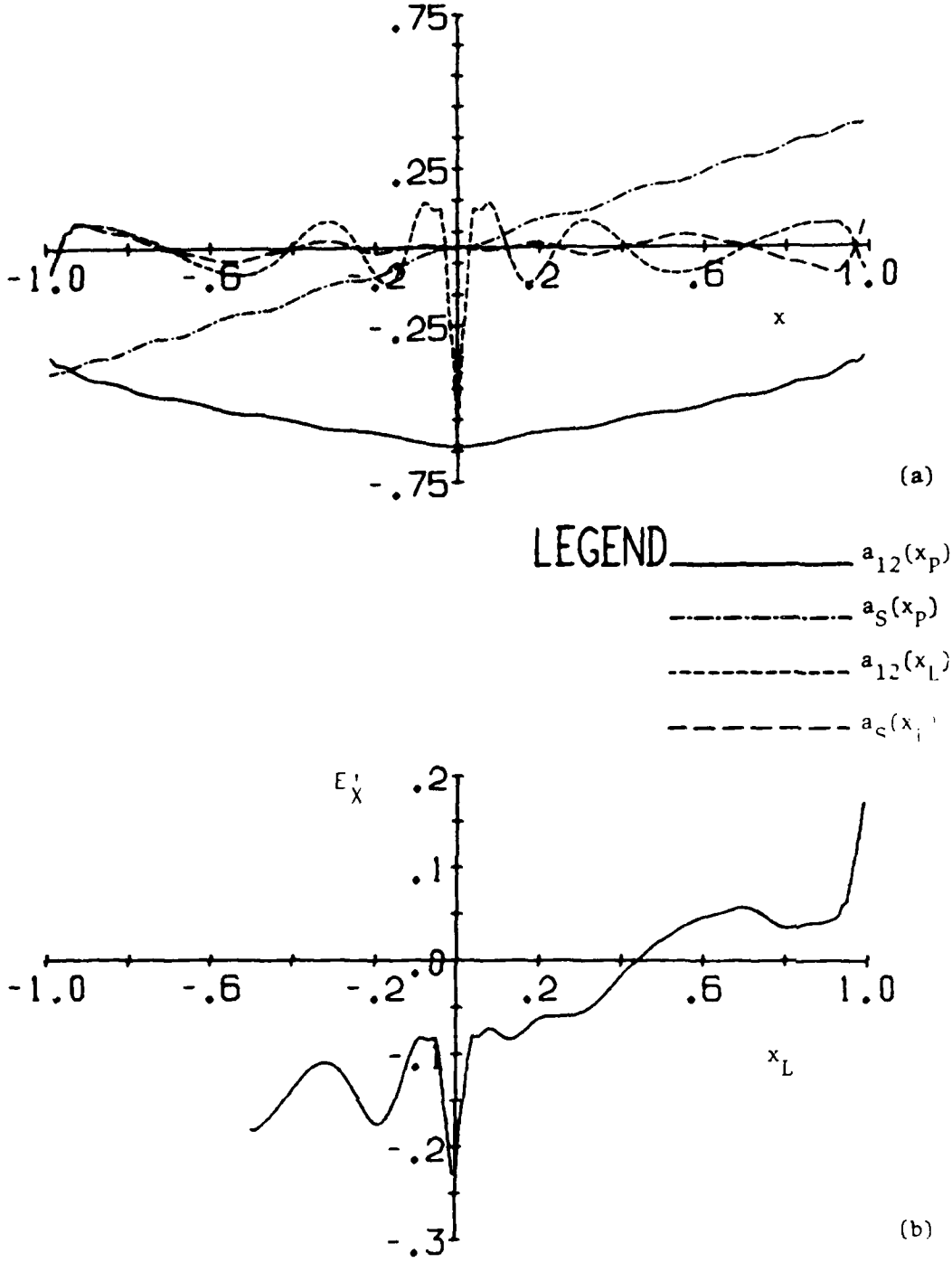

FIGURE 15 - Line and point images;
separation = 0.5, N = 1.0

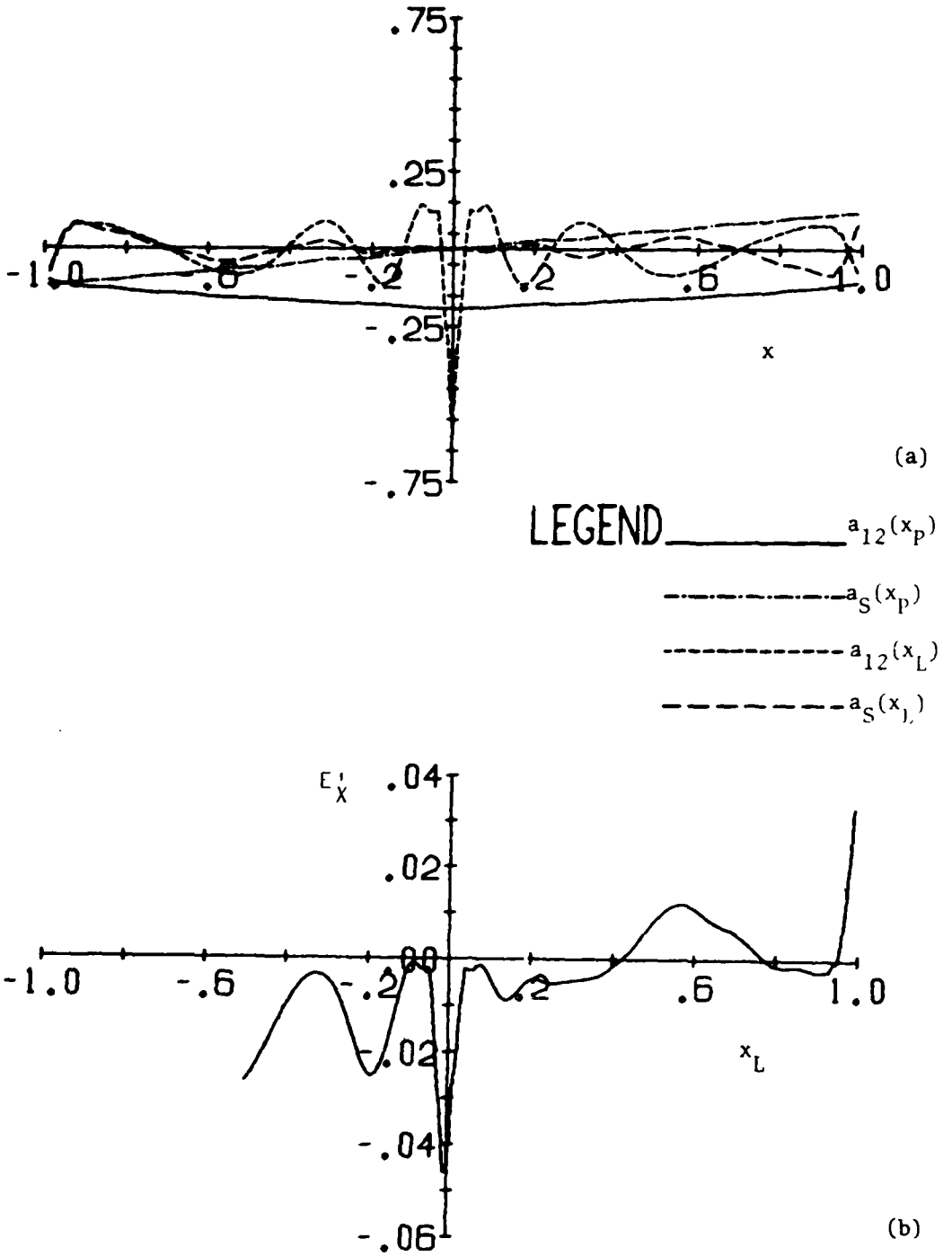

FIGURE 16 - Line and point images;
separation = 0.5, N = 0.3

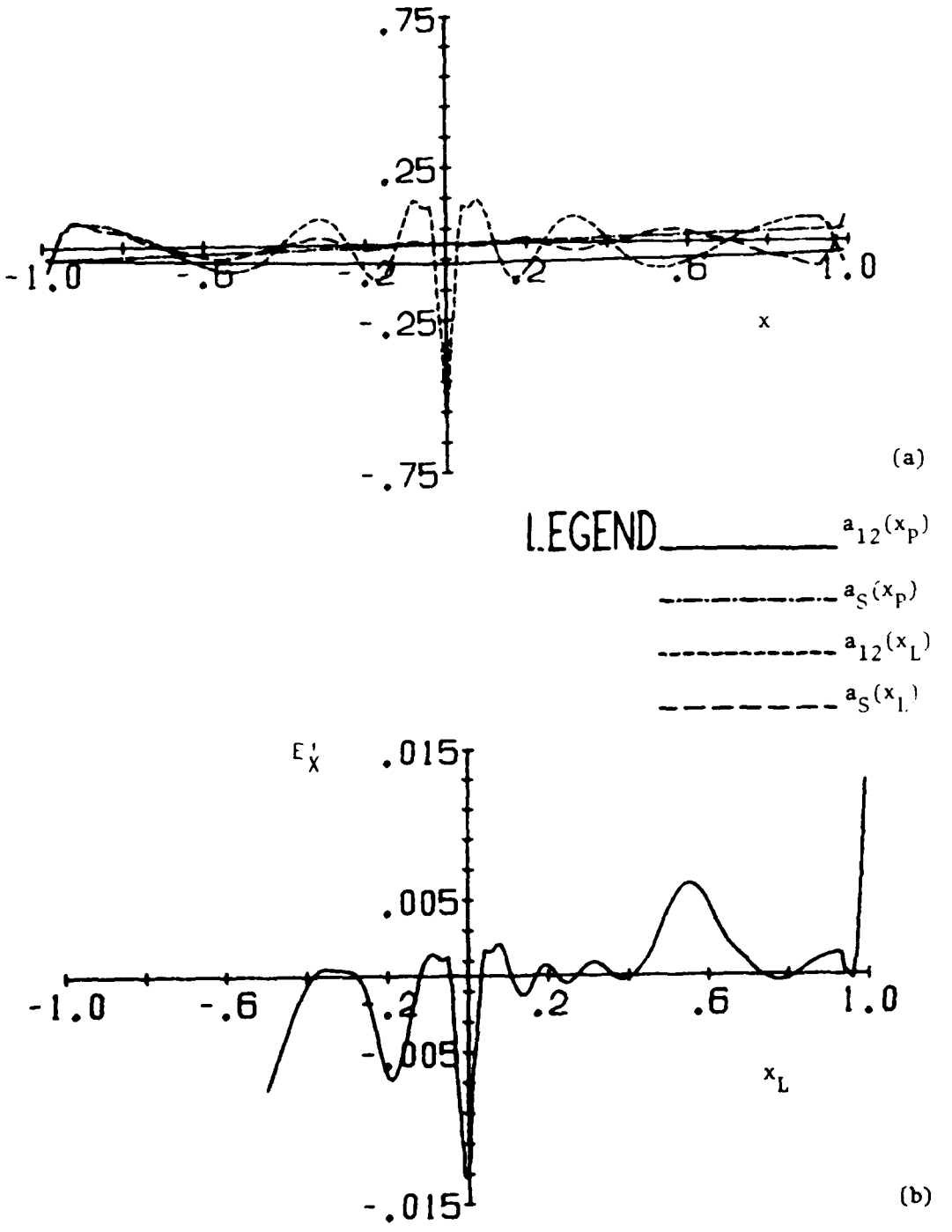

FIGURE 17 - Line and point images;
separation = 0.5, N = 0.1

Thus the equilibrium position can be given by the solutions of both

$$a_{12}(x_L - 0.5) + a_{12}(x_L) = 0 \ ,$$
$$a_S(x_L - 0.5) + a_S(x_L) = 0 \ . \qquad [28]$$

These equations could be solved by plotting the error signal, and noting the zero crossings. A positive slope at these positions would show stability, as a movement of the reticle centre to the left would be accompanied by a positive error signal, which would tend to return the reticle to its equilibrium position. Although the error signal can be very easily calculated, the value of RMS is involved, for which a_{11}, a_{12} and a_{13} are required. A more direct approach is to use the data from the curves of Figs. 15(a)-17(a), where only the a_{12}'s and a_S's are given. Let

$$E_X = E_X'/RMS^2 \ , \qquad [29]$$

Then because RMS^2 cannot be negative, E_X' must have the same zero crossings as E_X, and the signs of the slopes at these positions must be the same for E_X and E_X'. Thus, the equilibrium positions are determined by plotting E_X', where

$$E_X' = [a_{12}(x_L - 0.5) + a_{12}(x_L)]\,[a_S(x_L - 0.5) + a_S(x_L)] \ . \qquad [30]$$

In Figs. 15(b), 16(b) and 17(b) this curve is shown for N = 1.0, 0.3 and 0.1 respectively.

It can be seen for N = 1.0 that there is one equilibrium position, that it is stable, and occurs for $x_L = 0.43$, $x_P = -0.07$. For N = 0.3, there are three equilibrium positions, two of which are stable.

For N = 0.1, there are 15 equilibrium positions of which 8 are stable. The figures show that if a 41-point representation had been employed instead of a 21-point one, the larger carrier peak to the right of the ordinate might have caused two more equilibrium positions to have occurred at x_L's between 0 and 0.1, for N = 0.3.

4.0 DISCUSSION

In practice, a small portion of the centre of the reticle may be blacked out to prevent oscillation of the seeker when the error is small. This would change the shape of the two point target equilibrium curves in the region where one of the images enters this zero transmission zone.

Multiple statically stable equilibrium positions were found under certain conditions when both a point and a line image were present on the reticle. Under dynamic conditions some of these positions may not be stable.

The filters employed extracted the carrier and its immediate side-bands with no attenuation or phase shift. The simulation model could be readily adapted to filters requiring attenuation and phase shift at particular harmonics.

The only extended target examined was a line. However, areal targets, such as illustrated in Fig. 18, could be studied, but because of the large number of points required to define an areal target and the consequent large number of computer operations entailed, the programming would probably have to be performed in a language other than APL.

The reticle employed is the 'sunburst' reticle with straight spokes. Other reticles could be employed with very small changes to the simulation. One such reticle is illustrated in Fig. 19, in which the spiral spokes improve the spatial filtering.

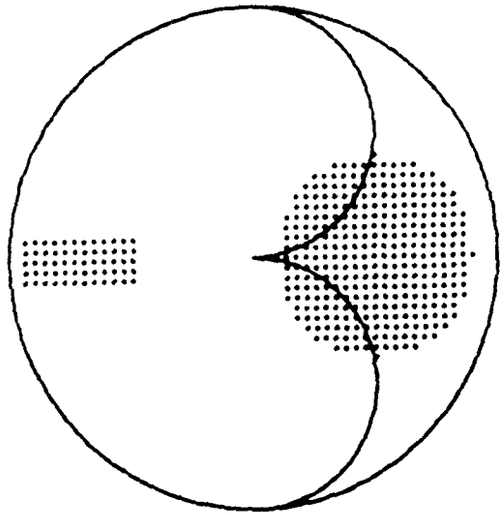

FIGURE 18 - Distributed targets

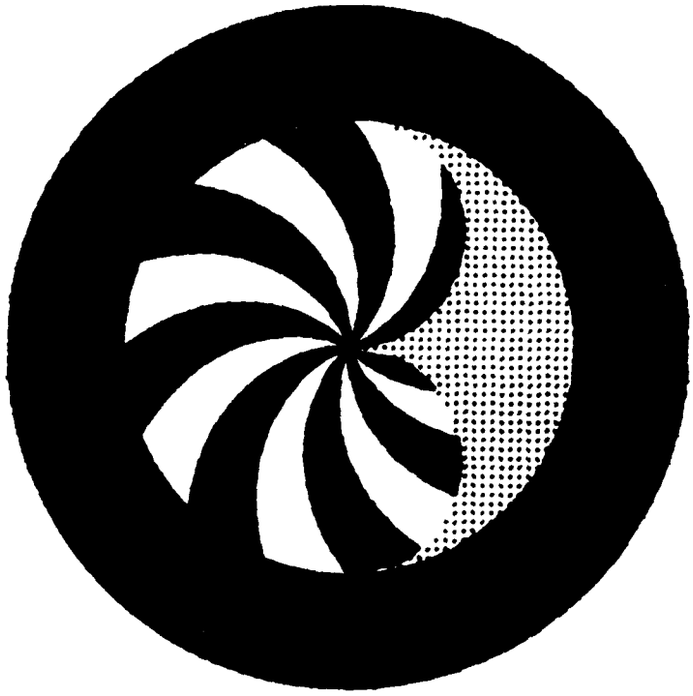

FIGURE 19 - Spiralled reticle

5.0 CONCLUSION

A simulation model of a generic seeker employing an AM reticle was developed, from which a digital programme was prepared to calculate the seeker response to various stimuli. It was demonstrated that the equilibrium position of two point images can be described by a weighted mean only if the separation and intensity ratio is such that neither image, at equilibrium, is nearer the reticle centre than 0.1 of the reticle radius. This occurs because the system is linear except for images near the centre of the reticle.

It was shown that, because of phase cancellations, an extended image contributes less to the error signal than a point of the same total intensity; hence a weighted mean cannot be used for determining the equilibrium position of an extended and a point image. The programme disclosed that with both a line and a point image present on the reticle, for certain ranges of intensity ratio, there could be many static equilibrium positions.

The model could be modified to accommodate the given characteristics of a particular AM reticle seeker, such as the geometry of the reticle, the amplitude and phase responses of the carrier filter, and the design of the automatic gain control. Areal targets of specified shapes and gradations in intensity could also be simulated.

APPENDIX A

Derivation of Equation 20

From Fig. 7

$$f(B,\alpha) = f(A, \alpha+\pi/12), \qquad [A1]$$

where

$$\alpha = \omega_s t .$$

It follows that

$$\begin{aligned}\int_0^{2\pi} f(B,\alpha)\sin 12\alpha \, d\alpha &= \int_0^{2\pi} f(A,\alpha+\pi/12)\sin 12\alpha \, d\alpha, \\ &= \int_0^{2\pi} f(A,\alpha)\sin(12\alpha - \pi) \, d\alpha, \qquad [A2] \\ &= -\int_0^{2\pi} f(A,\alpha)\sin 12\alpha \, d\alpha.\end{aligned}$$

Therefore

$$\begin{aligned}\int_0^{2\pi} f(A+B)\sin 12\alpha \, d\alpha &= \int_0^{2\pi} [f(A) + f(B)]\sin 12\alpha \, d\alpha \\ &= 0. \qquad [A3]\end{aligned}$$

Similarly

$$\int_0^{2\pi} f(A+B)\cos 12\alpha \, d\alpha = 0. \qquad [A4]$$

APPENDIX B

Derivation of the Constant in Equation 21

From Fig. 8

$$a_p = \frac{1}{\pi}\int_0^{2\pi} (\text{photocell signal})\sin p\alpha \, d\alpha,$$

$$= \frac{1}{\pi p}\sum_{i=0}^{6}(-1)^i\left[\cos\frac{(7+i)}{12}p\pi - \cos\frac{(6+i)}{12}p\pi\right], \qquad [B1]$$

$$= \frac{2}{\pi p}\left(1-\cos\frac{p\pi}{12}\right)\sum_{j=0}^{2}\cos(7+2j)\frac{p\pi}{12},$$

$$= \frac{2}{\pi p}\left(1-\cos\frac{p\pi}{12}\right)\cos\frac{9p\pi}{12}\left(1+2\cos\frac{2p\pi}{12}\right).$$

Therefore

$$a_{11} = 7.596/11\pi,$$
$$a_{12} = -1/\pi, \qquad [B2]$$
$$a_{13} = 7.596/13\pi.$$

APPENDIX C

Listing of Computer Programmes

Function QL2

```
      ∇OUT←QL2;I;G;A;P;Q;S;T;RMS
[1]    I←1
[2]    P←Q←0
[3]   MQ:T←((XX[I]×XX[I])+YY[I]×YY[I])*.5
[4]    →(T>1)/MT
[5]    G←ZZ[I]×QL1 XX[I],YY[I]
[6]    A←1 2∘.○G×FI
[7]    P←P+(G[1;]×A[2;])-G[2;]×A[1;]
[8]    Q←Q+(G[1;]×A[1;])+G[2;]×A[2;]
[9]   MT:→(I=⍴XX)/PX
[10]   I←I+1
[11]   →MQ
[12]  PX:RMS←(+/S×S←P,Q)*.5
[13]   P←P÷RMS
[14]   Q←Q÷RMS
[15]   S←+/¯1↓P×1⌽P
[16]   S←S++/¯1↓Q×1⌽Q
[17]   T←+/¯1↓Q×1⌽P
[18]   T←T-+/¯1↓P×1⌽Q
[19]   OUT←(-S),T
       ∇
```

Use: Calculates E_X and E_Y for any number of point images defined by the vector XX, YY and ZZ, where XX(I), YY(I) and ZZ(I) correspond to the position and intensity of the i'th image.

Calls: QL, QL1

Function QL1

```
      ∇G←QL1 RR;Y;P;Q;CO;E;TERM;N
[1]   Y←QL RR
[2]   P←Y[1;]
[3]   Q←Y[2;]
[4]   CO←1○P[1]×GG←(.5×N←24)÷(-1+⌊.5×TERM)÷⍳TERM←3
[5]   Y←(0,Q[1]=0)⌿Y
[6]   P←Y[1;]
[7]   E←⍉[1]⍉((⌊.5×⍴P),2)⍴P
[8]   G←+/[2]-/[2]2 1∘.○E∘.×GG
[9]   G[2;]←G[2;]+CO
[10]  G[1;]←-G[1;]
[11]  G←G⌽○(2,TERM)⍴GG
      ∇
```

Use: Determines a_i, b_i (i = 11, 12, 13) for a given point image

Calls: QL1

Called by: QL2

Function QL

```
      ∇Y←QL RR;R;X;Z;P;C;QQ;N
[1]   R←(+/RR×RR)*.5
[2]   FI←RR[1]ATAN RR[2]
[3]   X←(0÷.5×N)×0,¯1+N←24
[4]   X←(1,ρX)ρX
[5]   X←X,[1](,ρX)ρ0 1
[6]   X[1;]←X[1;]+(02)×P←X[1;]<0
[7]   X←(+/P)⌽X
[8]   X[1;]←X[1;]-(02)×P←X[1;]>02
[9]   Y←(-+/P)⌽X
[10]  Y←(0,((1↑ρY)ρ1),0)\Y
[11]  Y[1;1]←0
[12]  Y[1;1↑ρY]←02
[13]  Y[2;1]←1-Y[2;2]
[14]  Y[2;1↑ρY]←1-Y[2;¯1+1↑ρY]
[15]  Z←(0.5)-¯2○R
[16]  P←Y[1;]
[17]  C←P>Z
[18]  QQ←C⍳1
[19]  →(QQ=1)/AD
[20]  C[QQ-1]←1
[21]  Y←C/Y
[22]  Y[1;1]←Z
[23] AD:Z←(02)-Z
[24]  P←Y[1;]
[25]  C←P<Z
[26]  QQ←C⍳0
[27]  →(QQ>ρQ)/0
[28]  C[QQ]←1
[29]  Y←C/Y
[30]  Y[1;¯1↑ρY]←Z
      ∇
```

Use: Determines zero-crossing positions of the photocell waveform for a given point image.

Called by: QL1

Function MP

```
      ∇I←MP N;A;J;MO1;PO1
[1]   MO1←LINE[;2 3]
[2]   PO1←PIN[;2 3]
[3]   I←1
[4]   A←⍳0
[5]  AS:J←I+50
[6]   A←A,(MO1[I;1]+PO1[J;1]×N)×MO1[I;2]+PO1[J;2]×N
[7]   →(J=200)/AD
[8]   I←I+1
[9]   →AS
[10] AD:I←-A
      ∇
```

Use: Calculates the data for Figs 15(b), 16(b) and 17(b) from the matrices LINE and PIN, where LINE contains the values of $a_{12}(x_L)$ and $a_S(x_L)$ for $-1 \le x_L \le 1$, and PIN contains the values of $a_{12}(x_p)$ and $a_S(x_p)$ for $-1 \le x_p \le 1$.

Function ATAN

```
      ∇Z←X ATAN Y
[1]   →(1E¯6<|X)/U1
[2]   X←0
[3]   U1:Z←¯3○Y÷X+1E¯7
[4]   →(X<0)/YP
[5]   →AB
[6]   YP:Z←Z+○1
[7]   AB:Z←(○2)|Z
[8]   →(Z≤○1)/0
[9]   Z←Z-○2
      ∇
```

Use: Calculates the arctangent and assigns to it the appropriate value dependent on its quadrant.

CRDV R-4203/81 (NON CLASSIFIE)

Bureau - Recherche et Développement, MDN, Canada.
CRDV, C.P. 8800, Courcelette, Qué. G0A 1R0

"Poursuite de cibles multiples par un autodirecteur à réticule AM"
par K.W. Morgan

On a conçu un modèle mathématique de réticule de tête chercheuse à modulation d'amplitude et déterminé sa position d'équilibre stable en présence d'une cible à double points, ou à simple point accompagnée d'une cible étendue. Le comportement de ce réticule constitue l'objet d'une simulation sur ordinateur numérique. (NC)

CRDV R-4203/81 (NON CLASSIFIE)

Bureau - Recherche et Développement, MDN, Canada.
CRDV, C.P. 8800, Courcelette, Qué. G0A 1R0

"Poursuite de cibles multiples par un autodirecteur à réticule AM"
par K.W. Morgan

On a conçu un modèle mathématique de réticule de tête chercheuse à modulation d'amplitude et déterminé sa position d'équilibre stable en présence d'une cible à double points, ou à simple point accompagnée d'une cible étendue. Le comportement de ce réticule constitue l'objet d'une simulation sur ordinateur numérique. (NC)

CRDV R-4203/81 (NON CLASSIFIE)

Bureau - Recherche et Développement, MDN, Canada.
CRDV, C.P. 8800, Courcelette, Qué. G0A 1R0

"Poursuite de cibles multiples par un autodirecteur à réticule AM"
par K.W. Morgan

On a conçu un modèle mathématique de réticule de tête chercheuse à modulation d'amplitude et déterminé sa position d'équilibre stable en présence d'une cible à double points, ou à simple point accompagnée d'une cible étendue. Le comportement de ce réticule constitue l'objet d'une simulation sur ordinateur numérique. (NC)

CRDV R-4203/81 (NON CLASSIFIE)

Bureau - Recherche et Développement, MDN, Canada.
CRDV, C.P. 8800, Courcelette, Qué. G0A 1R0

"Poursuite de cibles multiples par un autodirecteur à réticule AM"
par K.W. Morgan

On a conçu un modèle mathématique de réticule de tête chercheuse à modulation d'amplitude et déterminé sa position d'équilibre stable en présence d'une cible à double points, ou à simple point accompagnée d'une cible étendue. Le comportement de ce réticule constitue l'objet d'une simulation sur ordinateur numérique. (NC)

CRDV R-4203/81 (NON CLASSIFIE)

Bureau - Recherche et Développement, MDN, Canada.
CRDV, C.P. 8800, Courcelette, Qué. G0A 1R0

"Poursuite de cibles multiples par un autodirecteur à réticule AM"
par K.W. Morgan

On a conçu un modèle mathématique de réticule de tête chercheuse à modulation d'amplitude et déterminé sa position d'équilibre stable en présence d'une cible à double points, ou à simple point accompagnée d'une cible étendue. Le comportement de ce réticule constitue l'objet d'une simulation sur ordinateur numérique. (NC)

CRDV R-4203/81 (NON CLASSIFIE)

Bureau - Recherche et Développement, MDN, Canada.
CRDV, C.P. 8800, Courcelette, Qué. G0A 1R0

"Poursuite de cibles multiples par un autodirecteur à réticule AM"
par K.W. Morgan

On a conçu un modèle mathématique de réticule de tête chercheuse à modulation d'amplitude et déterminé sa position d'équilibre stable en présence d'une cible à double points, ou à simple point accompagnée d'une cible étendue. Le comportement de ce réticule constitue l'objet d'une simulation sur ordinateur numérique. (NC)

CRDV R-4203/81 (NON CLASSIFIE)

Bureau - Recherche et Développement, MDN, Canada.
CRDV, C.P. 8800, Courcelette, Qué. G0A 1R0

"Poursuite de cibles multiples par un autodirecteur à réticule AM"
par K.W. Morgan

On a conçu un modèle mathématique de réticule de tête chercheuse à modulation d'amplitude et déterminé sa position d'équilibre stable en présence d'une cible à double points, ou à simple point accompagnée d'une cible étendue. Le comportement de ce réticule constitue l'objet d'une simulation sur ordinateur numérique. (NC)

CRDV R-4203/81 (NON CLASSIFIE)

Bureau - Recherche et Développement, MDN, Canada.
CRDV, C.P. 8800, Courcelette, Qué. G0A 1R0

"Poursuite de cibles multiples par un autodirecteur à réticule AM"
par K.W. Morgan

On a conçu un modèle mathématique de réticule de tête chercheuse à modulation d'amplitude et déterminé sa position d'équilibre stable en présence d'une cible à double points, ou à simple point accompagnée d'une cible étendue. Le comportement de ce réticule constitue l'objet d'une simulation sur ordinateur numérique. (NC)

DREV R-4203/81 (UNCLASSIFIED)

Research and Development Branch, DND, Canada.
DREV, P.O. Box 8800, Courcelette, Que. G0A 1R0

"Multiple target tracking with an AM reticle seeker"
by K.W. Morgan

A generic AM-reticle seeker was modelled, and its steady-state equilibrium position, in the presence of either two point targets or a point and an extended target, determined by digital computer simulation. (U)

DREV R-4203/81 (UNCLASSIFIED)

Research and Development Branch, DND, Canada.
DREV, P.O. Box 8800, Courcelette, Que. G0A 1R0

"Multiple target tracking with an AM reticle seeker"
by K.W. Morgan

A generic AM-reticle seeker was modelled, and its steady-state equilibrium position, in the presence of either two point targets or a point and an extended target, determined by digital computer simulation. (U)

DREV R-4203/81 (UNCLASSIFIED)

Research and Development Branch, DND, Canada.
DREV, P.O. Box 8800, Courcelette, Que. G0A 1R0

"Multiple target tracking with an AM reticle seeker"
by K.W. Morgan

A generic AM-reticle seeker was modelled, and its steady-state equilibrium position, in the presence of either two point targets or a point and an extended target, determined by digital computer simulation. (U)

DREV R-4203/81 (UNCLASSIFIED)

Research and Development Branch, DND, Canada.
DREV, P.O. Box 8800, Courcelette, Que. G0A 1R0

"Multiple target tracking with an AM reticle seeker"
by K.W. Morgan

A generic AM-reticle seeker was modelled, and its steady-state equilibrium position, in the presence of either two point targets or a point and an extended target, determined by digital computer simulation. (U)


DATE
ILME